Products of stopped-pion interactions with Cu and Ta

C. J. Orth, W. R. Daniels, B. J. Dropesky, R. A. Williams, and G. C. Giesler
Los Alamos Scientific Laboratory, Los Alamos, New Mexico 87545

J. N. Ginocchio
Theoretical Division, Los Alamos Scientific Laboratory, Los Alamos, New Mexico 87545

(Received 9 January 1980)

Yields of radioactive products from the interactions of stopped π^- with Cu and Ta have been measured. Absolute yields of products ranging down to 10^{-5} per stop were determined. The experimental yields are compared with yields calculated with a model that was developed in this work for the stopped-π^- interaction. The calculations give excellent agreement with measured total mass yields for Ta, but some discrepancies exist for the independent yields of Hf, Er, and Tm isotopes; in the case of Cu, most independent yields, except for Co and Sc, are in good agreement. Measurements were also made with both stopped π^- and 20-MeV π^+ on Cu and Fe to determine the shift in the centroids of the isotopic yields with pion charge.

[NUCLEAR REACTIONS Stopped-negative-pion interactions with Cu and Ta. Measured yields of residual radioactive products. Calculated yields from model for the interactions.]

I. INTRODUCTION

The process of stopped-pion absorption begins with the capture of a low-kinetic-energy π^- by the Coulombic potential of the nucleus. The capturing Bohr orbit is presumed to have a large principal quantum number n of about 20.[1] The resultant pionic atom deexcites by x-ray and Auger-electron emission until it reaches a lower n state with sufficient overlap of its wave function with the nuclear volume so that the nucleus captures the pion, due to the strong pion-nucleon interaction. In order to conserve momentum and energy the pion is presumed to be absorbed on at least a correlated pair of *pp* or *np* nucleons.

Absorption of the π^- converts a proton into a neutron, and the pion imparts its 140-MeV rest mass into kinetic energy of the absorbing pair, each nucleon of the pair recoiling in the center-of-mass system with about 70 MeV plus the original kinetic energy of the pair of nucleons. Depending on the point of absorption and the direction of motion of these recoiling nucleons, they can either escape without interaction or undergo collisions with other nucleons in the nucleus and thereby initiate an intranuclear cascade.

Early studies of the yields of radioactive products from the interactions of π^- with N, O, Zn, As, Br, I, and Hg targets have been reported by investigators at the University of Chicago.[2-7] Negative pions with initial kinetic energies of 30 to 70 MeV were stopped in very thick targets (~30 g/cm^2). Following irradiation, the different elemental products were chemically separated from the target material and the radioactivities were measured.

Gadioli and Gadioli-Erba[8] used an exciton model with fair success to fit the data of the Chicago authors. In this treatment the two nucleons that share the pion rest mass are assumed to give rise to two (parallel) intranuclear cascades, each characterized by a one-particle–one-hole initial configuration.

A rather sophisticated treatment of the stopped π^- process is reported by Iljinov, Nazaruk, and Chigrinov.[9] These authors assume a Gaussian form for the probability density of pion absorption with the nuclear radius corresponding to the center of the Gaussian as a variable parameter. The resultant intranuclear cascade is treated by a Monte Carlo method developed by Bertini[10] and the subsequent evaporation on the part of the excited nucleus is calculated by the method developed by Dostrovsky *et al.*[11] These authors[9] are able to duplicate the residual yields reported by the Chicago group[2-7] rather well. In addition, they reproduced measured neutron and charged-particle spectra.

A team at Dubna has measured the residual products from stopped-π^- interactions with some heavy targets ranging from Ta to Bi.[12,13] These researchers stress their observation of the production of high-spin products; however, most of their yields are reported on a qualitative basis.

A group at CERN has recently measured yields[14] from stopped-pion reactions in ^{9}Be, ^{10}B, ^{16}O, ^{31}P,

Ca, and ^{93}Nb. Also, a team at SIN has reported[15] on measurements of residual product yields using in-beam spectroscopy and activation methods on targets of ^{59}Co, ^{75}As, ^{197}Au, and ^{209}Bi.

Another recent investigation relevant to our study has been reported by a group[16] working at CERN on absolute yield measurements of high-spin states in Hf and Pb nuclei following pion capture in ^{181}Ta and ^{208}Pb. They measured prompt and delayed γ rays following the interaction and give absolute yields for quadrupole transitions in the even-even Hf isotopes from $A = 166$ to 178 with nuclear spins of the initial states as high as 16.

A primary aim of the present study was to provide information about the average depth of absorption of the pion and, possibly, about the mechanism of absorption, such as preference for absorption on *pp*, *np*, or either of these in clusters. We did this by measuring the yields of radioactive products from the interaction of stopped π^- with Cu and Ta targets and by comparing these data with model calculations. We measured about two dozen yields from each target, ranging from 10 to 10^{-3} percent per pion stop, thereby providing a rather stringent test of the calculations. In the model, the radial location of absorption is established by wave mechanical cascade calculations through use of an optical potential obtained from pionic x-ray measurements. To first order, the probability of absorption on *np* to *pp* pairs is equal to $2N/(Z-1)$. Upon absorption, the resulting intranuclear cascade is treated with the Monte Carlo code VEGAS[17,18]. The deexcitation of the residual nucleus following the cascade is calculated with the Dostrovsky, Fraenkel and Friedlander (DFF) evaporation code.[11]

II. EXPERIMENTAL

Stopped-π^- target exposures were performed at the low-energy pion channel (LEP) of the Clinton P. Anderson Los Alamos Meson Physics Facility (LAMPF). The channel was tuned for 170 MeV/*c* (80 MeV) π^- and the resultant beam composition, determined by dE/dx measurements, was 60% π^-, 36% e^-, and ~4% μ^-. The pions were slowed down to stop in the targets by degrading their energy with graphite plates. The exact thickness of graphite required to establish the maximum number of stops in the target foils was achieved by using a three-element $(12\bar{3})$ scintillator telescope coupled to conventional fast electronics. The differential range curves showed full width at half maximum (FWHM) = 2.4 g/cm^2 of graphite at any momentum bite $\Delta p/p$ between 0.2 and 2% due to pion straggle in traversing the ~12-cm thickness of degraders.

The targets were 3.8-cm diam disks of thin Cu or Ta stacked to a total thickness of ~1 g/cm^2. By using multiple-disk targets, we could apportion certain foils for various chemical procedures and direct counting, and by gross γ counting of each foil, we could also confirm the exact location of maximum pion stops per unit density. All counting was done in a low-background environment. The Cu targets were counted directly, while for the Ta targets, both direct counting and radiochemical separations before counting were performed. In the latter, Hf and four rare earth fractions (Er, Tm, Yb, and Lu) were separated. Most of the products emit γ rays which were measured with one of three different Ge(Li) detector systems. Photopeak intensities of the γ rays in the spectra were determined with the GAMANAL[19] computer code. Spectra were measured over a period of six months. The photopeak efficiencies of the detectors were determined with National Bureau of Standards ^{241}Am, ^{228}Th, and multiple-species sources. Two β-emitting products from Ta, ^{169}Er, and ^{170}Tm, were measured in a low-background proportional counter.

The absolute yields (atoms/pion stop) of several high-yield "monitor products" were determined for Cu and Ta from short-duration, low-intensity irradiations. The intensity was reduced by closing the momentum slits to $\Delta p/p \sim 0.1\%$ and the number of pion stops in each target was established by the use of the three-element $(12\bar{3})$ scintillator telescope. Under these conditions and with 225 μA on the 3-cm thick graphite pion production target, the stop rate was 7×10^4 sec^{-1}. In subsequent high-intensity pion irradiations, product yields down to 10^{-3}% were determined; the relative yields were converted to absolute values by normalization to the monitor products.

The contributions to product yields from secondary nucleon reactions (chiefly from neutrons) were estimated from measurements on secondary targets placed downstream of the primary targets. To ensure that the secondary target was beyond the range of the pions, a graphite absorber, 2 cm thick, was interposed between the primary and secondary targets.

Stopped muons can also contribute to the yields of products near the target via (μ^-, xn) and to a lesser extent via (μ^-, pxn) reactions. On the basis of reported stopped muon yields,[20,21] the larger range of muons than pions, and the 4% muon contamination in our pion beam, we estimate the muon contributions to ^{60,61}Co from Cu, and ^{179}Hf^m and ^{179}Lu from Ta to be less than 5% of the reported yields.

III. MODEL DESCRIPTION

The model used for calculating the yields of residual-spallation-product nuclei, resulting when stopped negative pions are absorbed in a target nucleus, has three steps. The initial step assumes that the pion is absorbed on two nucleons, thus transferring the pion rest energy to the two nucleons. In the next step these two recoiling nucleons can either escape or scatter from other nucleons and thereby transfer excitation energy to the nucleus. The third step involves particle evaporation from the heated nucleus, which yields the observed residual products.

The location of the pion absorption in the nucleus is calculated from pionic-atom data.[22] The wave function for each pionic orbit is determined by solving the Klein-Gordon equation with a pion-nuclear optical potential. This pion optical potential[23] has an imaginary part which is proportional to the square of the nuclear density due to the pion absorption on two nucleons. The strength of this absorptive potential is determined by fitting pionic x-ray transition strengths. The nuclear densities used in the pionic optical potential are taken from electron scattering.[24]

The resulting pion wave function has the form

$$\psi_l = \phi_l e^{iEt/\hbar}, \tag{1}$$

where ϕ_l is the radial wave function, E is the complex pion energy, and t is the time coordinate. The probability for absorption of the pion from each orbit is then calculated from the equation of continuity which determines that the pion is absorbed in a volume element, $dV = 4\pi r^2 dr$, where r is the distance from the center of the nucleus. We define the differential probability dP_l/dr for absorption of the pion from an orbit l along the radius r as

$$dP_l/dr = \frac{2\pi r^2 \hbar}{\mathrm{Im}E}\left(\vec{\nabla}\cdot\vec{j} - \frac{2\mathrm{Im}E\,|\phi_l|^2}{\hbar}\right), \tag{2}$$

where h is Planck's constant, $\vec{\nabla}$ is the gradient operator, and j_l is the pion current defined as

$$\vec{j}_l = \frac{i\hbar}{2m}(\phi_l \vec{\nabla}\phi_l^* - \phi_l^* \vec{\nabla}\phi_l)\,. \tag{3}$$

In order to calculate the total pion absorption probability, the relative weight W_l, with which a particular orbit l will be populated in the pionic-atom cascade must be estimated. This weighting was calculated by assuming that the pion was Coulomb captured in the atom with some initial distribution in angular momentum l_0 and then a Monte Carlo technique was used to follow the pion down through the pionic levels in order to determine the population of the final orbits.[25] Two simple distributions of initial angular momenta

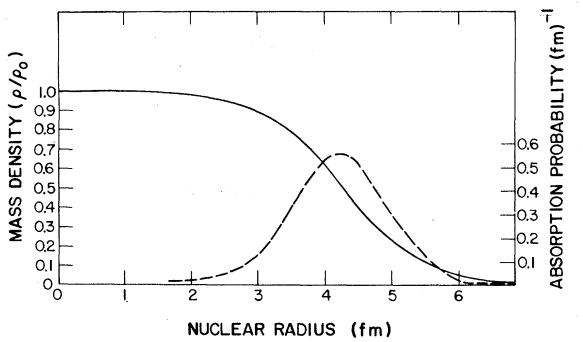

FIG. 1. The mass density for ^{63}Cu (solid line, left-hand scale) in units of the central density ρ_0 versus the nuclear radius. The mass density is from Ref. 24 and corresponds to a Fermi distribution with half radius = 4.2 fm and to a diffuseness = 0.59 fm. The absorption probability is plotted (right-hand scale) versus the radius.

were used, a uniform distribution and one proportional to the angular momentum degeneracy, $2l_0+1$. The total differential probability is then given by

$$dP/dr = \sum W_l\, dP_l/dr\,. \tag{4}$$

In Figs. 1 and 2, the absorption probability dP/dr is plotted for ^{63}Cu and ^{181}Ta for the initial distribution proportional to $2l_0+1$; the uniform initial distribution gives almost identical results. The capture probability shows a rapid rise from the

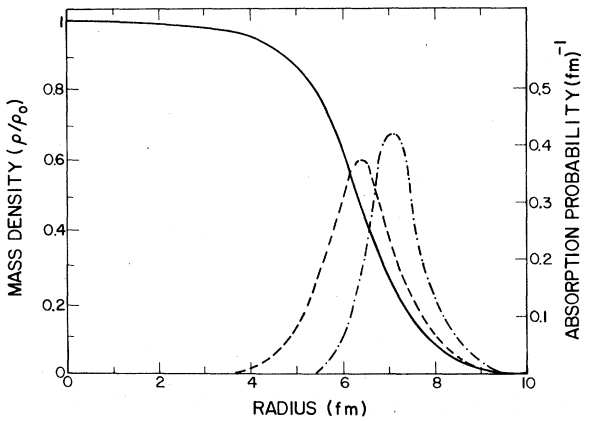

FIG. 2. The mass density for ^{181}Ta (solid line, left-hand scale) in units of the central density ρ_0 versus the nuclear radius. The mass density is from Ref. 24 and corresponds to a Fermi distribution with half radius = 6.4 fm and to a diffuseness = 0.64 fm. The absorption probability, calculated from the pionic-atom cascade code is shown dashed ($\rho/\rho_0 = 0.5$), while an arbitrarily chosen absorption distribution that peaks closer to the nuclear surface ($\rho/\rho_0 = 0.25$) is shown by the dash-dot curve.

edge of the nucleus, reaches a maximum at the half-central-density radius of the nucleus, and then slowly decreases to zero inside the nucleus. An arbitrarily chosen distribution for ^{181}Ta centered at the quarter-central-density radius is also shown in Fig. 2. This distribution is used to test the sensitivity of the model to the location of the pion absorption.

The negative pion can be absorbed on either a neutron-proton pair or a proton-proton pair. The probability that it will absorb on the neutron-proton pair will be proportional to the number of neutron-proton pairs in the nucleus NZ. The probability that it will absorb on a proton-proton pair will be proportional to the number of proton-proton pairs, $Z(Z-1)/2$. We define the ratio of these probabilities as the quantity R which then will be

$$R=2k\frac{NZ}{Z(Z-1)}=R_0\frac{N}{(Z-1)}, \tag{5}$$

where k is the proportionality constant. For convenience we have defined R_0 as

$$R_0=2k \tag{6}$$

so that $R\simeq R_0$ for $N=Z$ nuclei. From Eq. (5) we see that for absorption that is equally probable on neutron-proton pairs as well as on proton-proton pairs, $k=1$ or $R_0=2$.

The value of R_0 depends on the details of the pion absorption mechanism. For delta dominance, that is, absorption through a pion-nucleon isospin $\frac{3}{2}$ partial wave only, R_0 has a unique value of 5, independent of the magnitude of the absorption.[26] For absorption through a pion-nucleon partial wave with isospin $\frac{1}{2}$, R_0 can vary between 0 and 2. When both partial waves are contributing, there are no *a priori* bounds on R_0.

The quantity R_0 has a direct physical significance in that it represents the extent to which neutron-neutron pairs are ejected from the nucleus compared to neutron-proton pairs. As R_0 increases, π^- absorption will tend to produce more neutron-deficient isotopes because n-n out will result in a lower N/Z than for n-p out.

However, R_0 is not very well known. The experimental ratio of neutron-neutron pairs to neutron-proton pairs ejected from the nucleus, which we denote by R_e, has been measured for a number of nuclei.[27] If there were no charge-exchange scattering of the two nucleons as they leave the nucleus, R_e would be identical to R. However, charge-exchange scattering of the

TABLE I. Yields of products from stopped-π^- interaction with Cu.

Nuclide		Yield type	E_γ (keV)	γ/dis	Measured yield (%)	Calculated yield (%)
6.1 -d	^{56}Ni	*I*	751	0.474	0.0074±0.0030	0.008±0.008
36-h	^{57}Ni	*I*	1377	0.78	0.119 ±0.014	0.232±0.068
17.9-h	^{55}Cq	*C*	931	0.73	0.115 ±0.014	0.156±0.056
78.5-d	^{56}Co	*C*	847	1.00	1.41 ±0.12	1.46 ±0.17
271.4-d	^{57}Co	*C*	122	0.859	6.80 ±0.75	4.58 ±0.30
71.3-d	^{58}Co	*I*	811	1.00	11.3 ±1.2	7.90 ±0.40
5.26-y	^{60}Co	*I*	1173/1332	1.00/1.00	6.35 ±0.85	5.55 ±0.33
1.65-h	^{61}Co	*C*	67	0.90	2.71 ±0.40	2.89 ±0.24
8.3-h	^{52}Fe	*C*	168	1.00	0.0028±0.0004	0.002±0.002
44.6-d	^{59}Fe	*C*	1099/1292	0.562/0.432	1.37 ±0.15	2.19 ±0.21
5.63-d	^{52}Mn	*I*	1434	1.00	0.42 ±0.05	0.34 ±0.08
313-d	^{54}Mn	*I*	835	1.00	4.41 ±0.60	3.24 ±0.25
2.58-h	^{56}Mn	*C*	847	1.00	1.66 ±0.20	2.23 ±0.21
21.6-h	^{48}Cr	*C*	308	0.99	0.0011±0.0003	[a]
42-min	^{49}Cr	*C*	91	0.539	0.023 ±0.004	0.002±0.002
27.7-d	^{51}Cr	*C*	320	0.098	1.23 ±0.18	0.46 ±0.10
16.0-d	^{48}V	*C*	983	1.00	0.087 ±0.010	0.01 ±0.01
3.93-h	^{44}Sc	*I*	1157	1.00	0.0062±0.0008	[a]
58.6-h	^{44}Sc^m	*I*	1157	1.07		
83.8-d	^{46}Sc	*I*	889	1.00	0.056 ±0.009	0.004±0.004
3.35-d	^{47}Sc	*I*	159	0.73	0.041 ±0.008	0.018±0.018
43.7-h	^{48}Sc	*I*	1037	1.00	0.020 ±0.004	0.028±0.024
22.2-h	^{43}K	*C*	373	0.87	0.0029±0.0006	[a]
1.83-h	^{41}Ar	*C*	1294	0.99	0.0006	[a]
15.0-h	^{24}Na	*C*	1369	1.00	0.0037±0.0020	[a]

[a] No events occurred for these products in the calculations.

emerging nucleons will decrease this ratio[26] so that $R_e < R$. The experimental errors are large and can accommodate any value of R_0 ranging from 1.6 to 3.4. This uncertainty, coupled with $R_e < R$, does not fix R_0 very well. In this work, we have used predominantly the value $R_0 = 2$, which corresponds to absorption being equally probable on neutron-proton pairs as on proton-proton pairs.

In the present calculations, the two nucleons which absorb the pion are distributed uniformly in a momentum sphere with the Fermi momentum determined by the local density. The pion energy is transferred to the center of mass of the two nucleons, and the subsequent escape or collisions of the two nucleons with other nucleons is determined by the VEGAS intranuclear cascade model.[17,18] After the original two nucleons plus the subsequently struck nucleons escape or are captured by the average nucleon potential, a heated nucleus remains. This excited nucleus evaporates off neutrons, protons, deuterons, tritons, ^{3}He, and α particles, and the residual nuclei are the observed spallation products. The evaporation stage is calculated with the DFF (Ref. 11) evaporation code. Angular momentum effects are ignored in the evaporation calculation.

IV. RESULTS

The absolute yields of residual products from the interactions of stopped π^- with Cu and Ta are given in Tables I and II. The relative yields from the high-intensity target exposures were put on an absolute basis by normalization to several high-yield, nearly saturated, monitor products. For Cu, the monitors were ^{55}Co, ^{56}Mn, and ^{49}Cr, and for Ta they were ^{170}Hf, ^{171}Hf, and ^{172}Lu. The photopeak energies, branching ratios, and the half-lives of the radioactive products,

TABLE II. Yields of products from stopped-π^- interaction with Ta.

Nuclide		Yield type	E_γ (keV)	γ/dis	Measured yield (%)	Calculated yield (%)
16-h	^{170}Hf	*I*	165/621	0.35/0.23	4.2 ±0.7	0.98 ±0.14
12.2-h	^{171}Hf	*I*	662	0.15	5.1 ±0.7	2.48 ±0.22
1.9-y	^{172}Hf	*I*	1093	0.65	6.9 ±0.6	4.76 ±0.31
23.6-h	^{173}Hf	*I*	124	0.995	9.0 ±1.5	6.62 ±0.36
70-d	^{175}Hf	*I*	343	0.82	11 ±0.7	8.50 ±0.41
52-min	^{177}Hf^m	*I*	277	0.93	0.068 ±0.020	<5.2
29-d	^{179}Hf^m	*I*	363/454	0.39/0.67	0.31 ±0.06	<3.6
55-min	^{167}Lu	*I*	239	0.12	0.028 ±0.009	0.026±0.023
1.42-d	^{169}Lu	*C*	960	0.237	3.0 ±0.3	1.10 ±0.16
2.02-d	^{170}Lu	*I*	987	0.067	2.3 ±0.25	2.60 ±0.23
8.22-d	^{171}Lu	*I*	741	0.527	3.26 ±0.31	3.98 ±0.28
6.70-d	^{172}Lu	*I*	1093	0.65	3.33 ±0.36	5.26 ±0.32
512-d	^{173}Lu	*I*	271	0.22	3.6 ±0.35	5.10 ±0.32
142-d	^{174}Lu^m	*I*	67.1	0.16	3.7 ±0.4	5.11 ±0.32
1204-d	^{174}Lu^g	*I*	76.5			
3.69-h	^{176}Lu^m	*I*	88.4	0.087	1.2 ±0.2	3.1
6.61-d	^{177}Lu^g	*I*	208	0.0994	1.55 ±0.22	1.88 ±0.19
160-d	^{177}Lu^m	*I*	208	0.04		
23-min	^{178}Lu^m	*I*	426	0.95	0.27 ±0.11	1.3
4.6-h	^{179}Lu	*I*	214	0.123	0.28 ±0.04	0.36 ±0.08
56.7-h	^{166}Yb	*C*	82	0.15	0.45 ±0.12	0.058±0.034
31-d	^{169}Yb	*C*	198	0.36	4.4 ±0.5	2.28 ±0.30
4.21-d	^{175}Yb	*I*	396	0.065	0.34 ±0.04	0.33 ±0.08
1.9-h	^{177}Yb	*I*	150	0.22	0.018 ±0.003	0.076±0.039
30.6-h	^{165}Tm	*C*	243	0.433	0.11 ±0.013	0.026±0.023
7.70-h	^{166}Tm	*I*	778	0.20	0.079 ±0.018	0.144±0.054
9.29-d	^{167}Tm	*C*	208	0.403	1.1 ±0.1	0.77 ±0.21
93-d	^{168}Tm	*I*	816	0.482	0.13 ±0.02	0.50 ±0.10
126-d	^{170}Tm	~*I*	β^-		0.10 ±0.01	0.39 ±0.09
63.6-h	^{172}Tm	~*I*	1093	0.060	0.028 ±0.004	0.13 ±0.05
8.24-h	^{173}Tm	~*I*	399	0.806	0.013 ±0.003	0.096±0.044
9.3-d	^{169}Er	~*I*	β^-		0.0043±0.0006	0.040±0.028
7.52-h	^{171}Er	~*I*	308	0.658	0.0012±0.0002	0.012±0.012

used in the yield calculations, are included in the tables. Cumulative or independent yields are denoted by C or I.

The experimental errors quoted in the tables are due chiefly to uncertainties in photopeak intensity measurements. Smaller error contributions arise from corrections for photon absorption in the target foil, extended source geometry, and detector photopeak efficiency. The quoted errors do not include a possible systematic uncertainity, estimated to be less than ±12%, due to the determination of pion stops in the absolute yield measurements. In the calculations, 5000 stops were followed and the errors are statistical, ranging from ±5% for yields of about 10% to ±50% for yields near 0.1%.

The experimental independent yields of products from Cu are plotted in Fig. 3 and compared with calculations; smooth curves are drawn through calculated yields to guide the eye.

For Ta, measured independent yields are compared with calculations in Figs. 4 and 5. Smooth curves have been drawn through the calculated points to guide the eye. In the case of Ta, we were able to measure about two thirds of the total mass yields, compared to about 38% of the total for Cu. We have estimated the missing Ta yields (mainly the stable isotopes) by applying the computer code RUDSTAM[28] to our measured data. This code was developed at Brookhaven to calculate missing spallation product yields, using Rudstam's original empirical formulation.[29] The resultant total mass yields for Ta are compared with the stopped-pion model calculations in Fig. 6.

Contributions to the observed yields due to secondary reactions can be estimated by measuring Z (Cu) and $Z+1$ (Zn) radioactivities in the Cu target foils and in secondary target foils placed downstream behind sufficient absorber so they are beyond the range of the pions. The Z and $Z+1$ products are unique to secondary reactions because π^- absorption leads to species with $Z < 29$. These statements apply equally well to the Ta targets.

The results of measurements of secondary reaction products are given in Table III. In Cu, (p, xn), (n, xn), (n, p), and (n, spall) products were detected, while in Ta only (n, xn) and (n, p) products were observed. Products due to (n, α) reactions $(Z-2)$ were not observed in the secondary targets; however, contributions from this

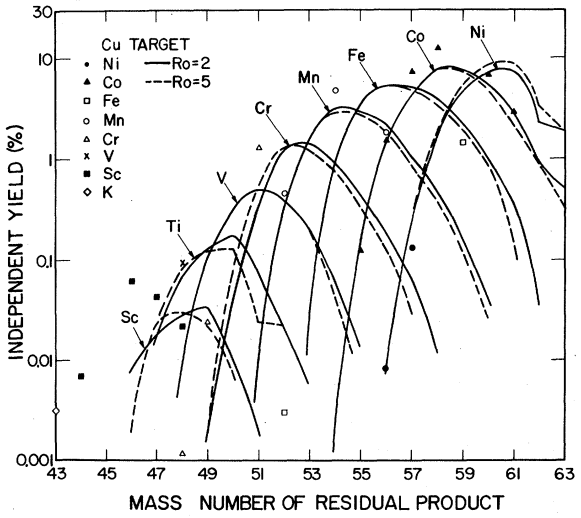

FIG. 3. Independent yields of residual spallation products from stopped-π^- interactions with Cu. Experimental values are shown as points and smooth curves are drawn through the calculated points (not shown). The solid and dashed curves are for $R_0=2$ and 5, respectively, where R_0 is the ratio of the probabilities for absorption on an n-p pair to absorption on a p-p pair.

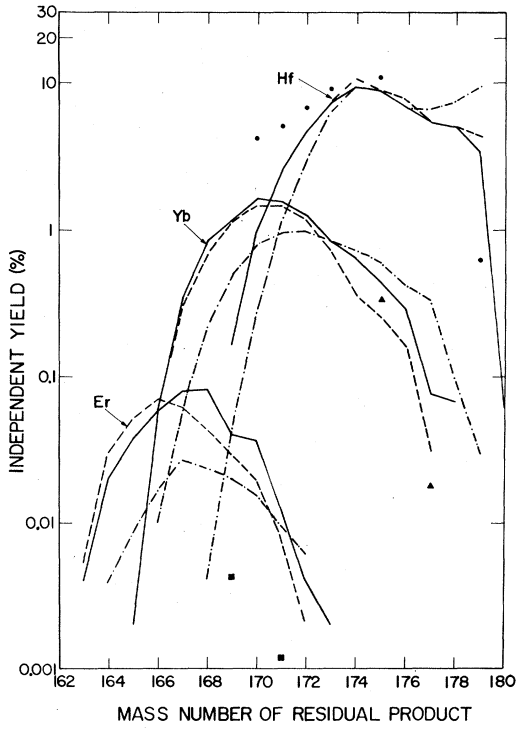

FIG. 4. Independent yields for residual Hf, Yb, and Er products from the interaction of stopped π^- with Ta. The measured yields are shown as circles (Hf), triangles (Yb), and squares (Er). Curves are established from the calculated yields. Solid and dashed curves are for $R_0=2$ and 5, respectively. The dash-dot curves are for $R_0=2$, but with an absorption probability arbitrarily peaked closer to the nuclear surface (see Fig. 2). The measured yield for ^{179}Hf represents a lower limit because only the high-spin isomer was detectable.

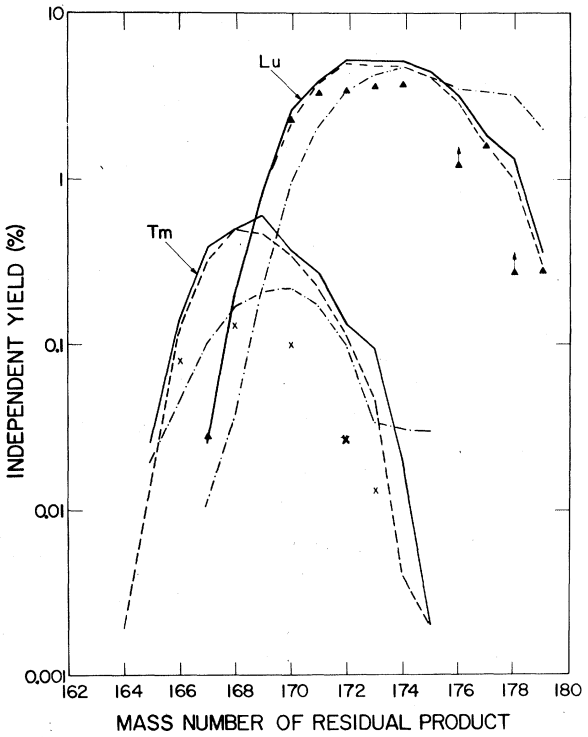

FIG. 5. Independent yields for residual Lu and Tm products from the interaction of stopped π^- with Ta. The measured yields are shown as triangles (Lu) and crosses (Tm). Curves are established from the calculated yields. Solid and dashed curves are for $R_0 = 2$ and 5, respectively. The dash-dot curves are for $R_0 = 2$, but with the absorption probability arbitrarily peaked closer to the nuclear surface (see Fig. 2).

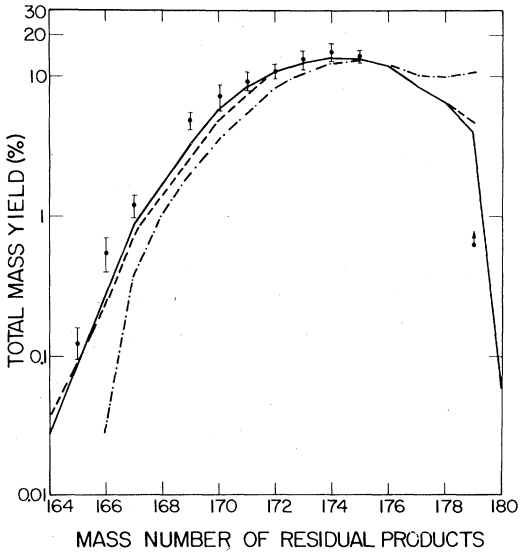

FIG. 6. Total mass yields for residual products from the interaction of stopped π^- with Ta. The points are the sums of experimentally determined yields with estimates of missing yields from the semi-empirical fitting routine described in Sec. IV. The smooth curves are established from the calculated yields. The solid and dashed curves are for $R_0 = 2$ and 5, respectively. The dash-dot curve is for $R_0 = 2$, but with the absorption probability peaked closer to the nuclear surface (see Fig. 2). The $A = 179$ yield is shown as a lower limit because only the high-spin isomer of ^{179}Hf was detectable.

reaction were estimated by comparing published (n, α) cross sections with $(n, 2n)$ or (n, p) excitation functions in the 8- to 20-MeV region. In Table III the yield per pion stop of ^{60}Co from the (n, α) reaction is estimated to be 0.1% which is to be compared with a total measured ^{60}Co yield of 7.05% per pion stop; this is about a 1.5% contribution from the secondary reaction. Presumably, about the same amount of (n, α) contribution occurs in Ta adding to the ^{178}Lu yield.

Due to the combination of low reaction cross sections and poor geometry, the only $Z < 29$ product we detected in the secondary Cu target foils was ^{56}Mn, presumably due to high-energy nucleon-induced spallation. The other $Z < 29$ species observed from the stopped π^- interactions must also be made to some extent by the high-energy secondary nucleons, but our measure-

TABLE III. Yields of products from secondary reactions.

Product	Cu target Yield (% per π^- stop)	Predominant reaction	Product	Ta Target Yield (% per π^- stop)	Predominant reaction
^{62}Zn	0.014	^{63}Cu$(p, 2n)$	^{178}Ta^m	0.22	$(n, 4n)$
^{63}Zn	0.052	^{63}Cu(p, n)	^{176}Ta	0.14	$(n, 6n)$
^{61}Cu	0.23	^{63}Cu$(n, 3n)$	^{181}Hf	0.040	(n, p)
^{64}Cu	0.64	^{65}Cu$(n, 2n)$	^{178}Lu	0.012 (est)	(n, α)
^{65}Ni	0.047	^{65}Cu(n, p)			
^{60}Co	0.10 (est)	^{63}Cu(n, α)			
^{62}Co	0.05 (est)	^{65}Cu(n, α)			
^{56}Mn	0.015	Cu $(n,$ spall)			

ments indicate that these contributions amount to about 1% and, therefore, are negligible for the ~1 g/cm^2 targets.

During the course of this work several measurements were made with Fe and Cu targets in order to determine the difference in residual product distributions when the charge on the incoming pion was changed from minus to plus. Of course, a positively charged pion cannot be Coulomb captured by a nucleus and must have sufficient kinetic energy to overcome the Coulomb barrier. For these measurements the π^+ were degraded with 4.45-cm-thick graphite plates, from an incident energy of 50 MeV down to about 20 MeV at the center of the target foil. Since the interaction cross section for π^+ drops rapidly with decreasing energy, below 100 MeV, we adopted a π^+ energy of 20 MeV for this comparison, although this energy is considerably higher than the Coulomb barrier. At 20 MeV, the π^+ interaction is predominantly absorption and inelastic scattering is relatively unimportant. The small amount of kinetic energy which can add to the pion rest-mass energy (140 MeV) upon absorption should not alter the π^+ yield distributions to any measurable degree.

The Mn and Co yields from Cu are shown in Fig. 7. For Co the shift is about 1.2 mass units. However, for Mn the shift is only about one half this amount; the reason for this smaller shift is not obvious.

In order to utilize the set of five measurable Sc isotopes to determine the extent of the shift expected due to changing the charge of the incoming pion, Fe was selected for the target material. Cu was not as suitable a target since the expected ^{61}Cu product from secondary nucleon reactions would preclude a determination of the ^{43}Sc yield. This is because ^{61}Cu has a strong γ transition in its decay which is identical in energy to the 373-keV γ ray of ^{43}Sc. The Sc yields from Fe, shown in Fig. 8, illustrate the shift in yield distributions between absorption of π^+ and π^-; here the shift in the centroids is again about 1.2 mass units. Although not shown here, measurements from a 20-MeV π^+ irradiation of Cu, compared with stopped-π^- results, indicate that from those Sc isotope yields that could be determined unambiguously, a shift of about 1.2 mass units occurs in the estimated centroids.

The centroid shifts in cross sections of Co, Mn, and Sc isotopes from fast π^+ and π^- reactions with Cu are, as one would expect, considerably smaller. The ΔA values decrease from 0.6 to approximately 0.2 mass units in going from 100 to 350 MeV.[30]

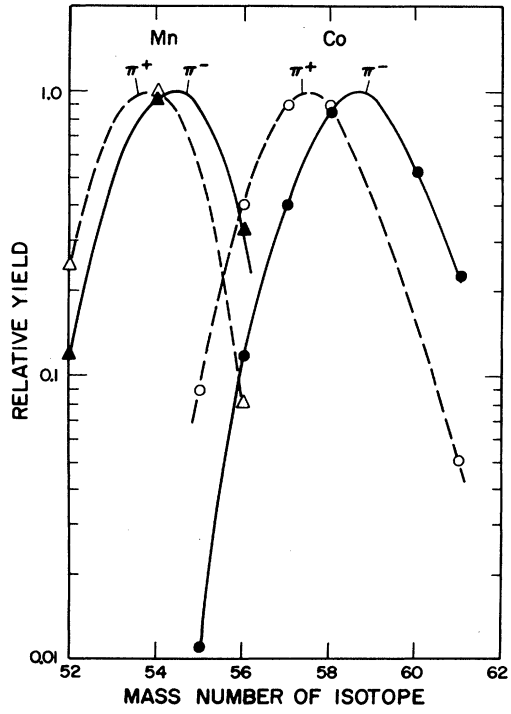

FIG. 7. Relative yields of Co and Mn spallation products from stopped π^- (solid points) and 20-MeV π^+ (open points) incident on Cu. The centroids are normalized to unity for easier comparison.

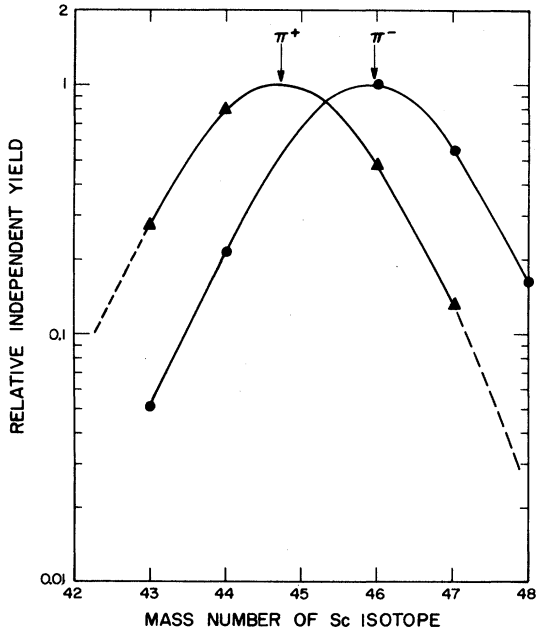

FIG. 8. Relative yields of Sc isotopes from stopped π^- (circles) and 20-MeV π^+ (triangles) incident on Fe. The centroids are normalized to unity for easier comparison.

V. DISCUSSION

A. Comparison of measured and calculated yields

For the independent yields shown in Fig. 3, those for cobalt are underestimated by the model. The greatest discrepancies, however, are the underestimations of the Cr, V, and Sc isotopic yields. Increasing the ratio R_0 from 2 to 5 does not change these results; the model does not seem to deposit enough energy in the Cu nucleus.

The agreement of the calculations with the measured total yields from Ta (Fig. 6) is quite good, although the products far removed from the target are somewhat underestimated. The experimental data for products near the target are less complete for comparison purposes. In Figs. 4 and 5, the individual isotopes are compared and we see a different situation than for copper. Only the isotopes of Hf, far removed from the target, are underestimated. The isotopes of Lu and Yb are predicted fairly well, but those of Tm and Er are severely overestimated. Changing R_0 from 2 to 5 does not significantly affect the calculated yields. We have also calculated the products with a pion absorption distribution which is peaked farther out on the edge of the nucleus, where the density is 25% of central density. This distribution, given in Fig. 2, improves the results for Tm and Er but gives poor results for the remaining isotopes.

The results on Cu and Ta indicate that the basic absorption mechanism used may not be the only mechanism involved. The neutron-deficient isotopes are being underestimated. The flatness of the Hf isotope curve and the low yields of the Tm and Er isotopes are difficult to reconcile in a simple model of pion absorption.

B. Comparison with previous studies

We show in Table IV a comparison of our ^{181}Ta results with yield data for stopped-π^- absorption in ^{181}Ta and nearby heavy nuclei, as reported by other investigators. The mean numbers of emitted neutrons and protons ($\langle n\rangle$ and $\langle p\rangle$) that we calculate for ^{181}Ta are very similar to those for ^{197}Au and ^{209}Bi reported by Pruys *et al.*[15] Also, these authors presented systematics that showed the centroids of the isotopic yield distributions (Gaussians) for (π^-, xn) products remain constant at $x \approx 6$ for $A = 165$ to 209, and the FWHM of all isotopic yield curves increase with target mass number. Our data for ^{181}Ta fit these systematics rather well. However, when we compare our data with those of Beetz *et al.*[16] for ^{181}Ta we find rather poor agreement. Why this is so we cannot say for certain, although, we suspect it may be due in part to the complexity of the prompt γ-ray spectrum in the 200-keV energy region. They report[16] absolute yields (per π^- stop) for the $4^+ \rightarrow 2^+$ γ transitions in the ground-state rotational bands of the even-even Hf isotopes. We note, for example, that the 207.4-keV $\frac{7}{2}^+[633] \rightarrow \frac{5}{2}^-[523]$ γ transition in high-yield ^{175}Hf might enhance the 206.5-keV photopeak from ^{174}Hf; the Table of Isotopes lists many γ rays in this energy region for the odd-mass Hf isotopes.

In the case of Cu, where we measured only 38% of the mass yield, we find that after correcting for the two isotopes of natural copper, the yield distributions are quite similar to those for ^{59}Co and ^{75}As reported by Pruys *et al.*[15], and the FWHM for the Mn and Co isotopic yield distributions (2.8 mass units) fit their systematics quite well.

C. Angular momentum considerations

The angular momentum brought into the nucleus by the Coulomb captured π^- is quite small since the pion itself has zero spin and only the pionic orbital momentum can be transferred. A large amount of angular momentum, however, can be imparted to the nucleus when a pion is absorbed near the surface and one of the absorbing nucleons escapes without further interaction, while the other nucleon, through collisions with other nucleons in the nucleus, imparts its kin-

TABLE IV. Comparison of isotopic yield data for π^- absorption in heavy nuclei.

Target	Centroid of (π^-, xn) isotopic yield (x)	FWHM of isotopic yield curves (ΔA)	$\langle n\rangle$	$\langle p\rangle$
^{165}Ho (Ref. 31)	6	6.1		
^{175}Lu (Ref. 31)	7	7.0		
^{181}Ta (Ref. 16)	8	5.2		
^{181}Ta (this work)	6	7.3	6.4 ± 0.5	0.40 ± 0.16
^{197}Au (Ref. 15)	6	8.9	6.6 ± 0.4	0.32 ± 0.14
^{209}Bi (Ref.15)	6	8.9	6.8 ± 0.4	0.37 ± 0.16
^{209}Bi (Ref. 16)	6	8.0		

TABLE V. Isomer ratios for ^{174}Lu and ^{177}Lu from ^{181}Ta.

Product	$I^{\pi}(m)/I^{\pi}(g)$	100-MeV protons	500-MeV protons	Stopped π^-
^{174}Lu	$6^-/1^-$	0.65±0.08	0.65 ±0.07	0.69±0.07
^{177}Lu	$\frac{23}{2}^-/\frac{7}{2}^+$	0.19±0.12	0.088± 0.030	0.15±0.04

etic energy to the nucleus. This twisting of the nucleus can transfer about 11 $\hbar$ units of angular momentum in Cu if the two nucleons recoil perpendicularly to a radius vector near the nuclear surface. Conversely, if a pion is absorbed deep in the nucleus, on the average, very little angular momentum will be imparted by the recoiling pair of nucleons, although much larger nuclear excitation energy will result compared with surface absorption.

Several authors[12,13] have emphasized the observed production of high-spin isomers of residual products by the stopped-pion interaction. Our measurements agree with this observation; however, we wish to point out the fact that this production of high-spin isomers is about the same as that which would be observed if the target nucleus were irradiated with ~70-MeV nucleons. One can visualize essentially the same impact parameters for 70-MeV nucleon-induced reactions and for stopped-π^- interactions near the nuclear surface.

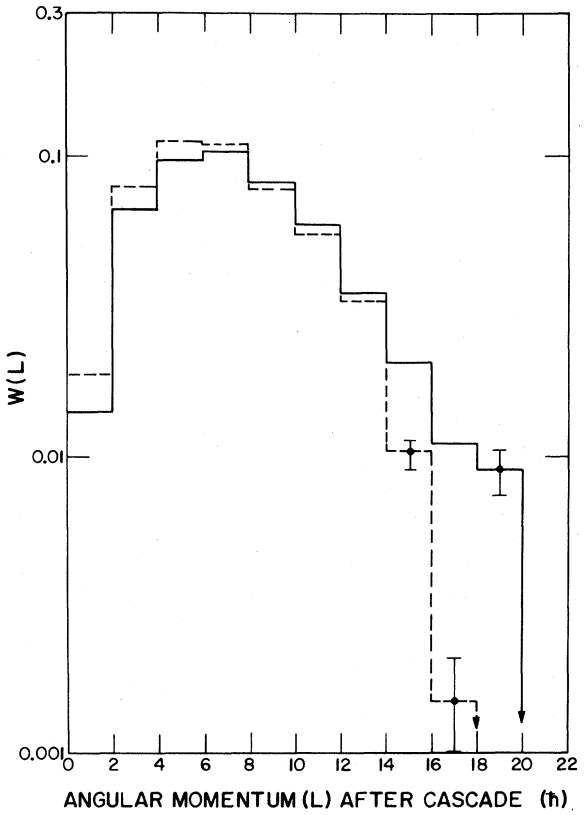

FIG. 9. The distributions of calculated angular momenta left in residual-product nuclei after the intranuclear cascade process for 70-MeV protons (solid line) and for stopped π^- (dashed line) incident on ^{181}Ta.

We have determined isomer ratios in ^{174}Lu and ^{177}Lu from stopped-π^- and 100- and 500-MeV proton reactions with Ta, and the data are given in Table V. The nuclear spin difference in the ^{174}Lu isomers is not very large and considerable particle evaporation occurs to erode the effect; however, the spin difference for the ^{177}Lu isomers is large, and these isomers lie within a few mass numbers of the ^{181}Ta target. Our measurements show, within the rather large uncertainties, that the isomer yields from stopped-π^- reactions with Ta are about the same as for fast-proton reactions. The fact that the isomer ratios are about the same for both 100- and 500-MeV protons and for stopped pions indicates that 70-MeV nucleons have essentially saturated the population of spin states with $\Delta I \leq 8$. This would probably not be the case if ΔI were much larger.

Angular momentum calculations using the stopped-pion interaction model and the VEGAS code for 70-MeV protons indicate that the angular momentum transfers to ^{181}Ta are very nearly the same for both projectiles. The calculated results are shown in Fig. 9.

VI. CONCLUSIONS

The data from this study are consistent with the smoothly increasing widths of the isotopic yield distributions with target mass number, and with a maximum in the (π^-, xn) yield distributions at $x=6$ for heavy mass targets, discussed in Ref. 15.

The stopped-pion interaction model discussed in Sec. III reproduces the experimental data fairly well. In the case of the Cu target it appears to underestimate the yields below $A=54$, suggesting that these calculations put too little excitation energy into the nucleus, and that the absorption of the pion occurs deeper, on the average, in the Cu nucleus than the model predicts. Also, when we compare the calculated yields with the measured independent yields given in Fig. 3, we notice that the measured yields for Sc iso-

topes peak near $A \approx 45$ while the calculations show the maximum near $A \approx 47$. This may be due to a deficiency in the DFF (Ref. 11) evaporation code which appears to overreact to the $N = 28$ neutron shell in both fast-pion and proton reaction studies.

Although for Ta the calculated total mass yields reproduce the observed yields quite well, there is considerable room for improvement in the calculated independent yields shown in Figs. 4 and 5. A new, more sophisticated evaporation code (JULIAN) has been written by Hillman and Eyal,[32] and its substitution for the DFF code may improve the agreement in the independent yield calculations for products many mass numbers removed from the target mass.

Comparisons of our experimental and calculated spallation-product yields indicate that the latter are rather insensitive to R_0, the ratio of pion absorption on n-p to p-p pairs. On the other hand, the calculated yields are quite sensitive to the radial depth of absorption, with the calculated half-central-density radius providing the best fit in Ta. In the case of Cu a slightly deeper absorption distribution than calculated would provide a better fit for the product yields.

Our measurements indicate that high-spin isomers are produced by π^- absorption in ^{181}Ta. However, both our measurements of isomer ratios in ^{177}Lu from ^{181}Ta targets irradiated with stopped π^- and with fast protons and our angular momentum calculations with the stopped-pion interaction model and the VEGAS code for 70-MeV protons, indicate that the angular momentum transfers to ^{181}Ta are very nearly the same for both projectiles.

From the results of the investigation of the influence of pion charge on the product yield distributions from Cu, the "memory" effect is clearly exhibited in yields of products from 2 to at least 8 units of Z from the target.

ACKNOWLEDGMENTS

We gratefully acknowledge the work of the LAMPF technical staff and operating crews for enabling the target exposures to be carried out. We thank G. A. Cowan and J. E. Sattizahn for their encouragement and support of this study. This work was performed under the auspices of the U.S. Department of Energy.

[1] J. Hüfner, Phys. Rep. 21C, 1 (1975).
[2] A. L. Turkevich and J. B. Niday, Phys. Rev. 84, 1253 (1951).
[3] T. T. Sugihara and W. F. Libby, Phys. Rev. 88, 587 (1952).
[4] A. L. Turkevich and S. Fung, Phys. Rev. 92, 521 (1953).
[5] A. L. Turkevich and J. B. Niday, Phys. Rev. 90, 342 (1953).
[6] N. Sugarman and A. Haber, Phys. Rev. 92, 730 (1953).
[7] L. Winsberg, Phys. Rev. 95, 198 (1954).
[8] E. Gadioli and E. Gadioli-Erba, Nucl. Phys. A256, 414 (1976).
[9] A. S. Iljinov, V. I. Nazaruk, and S. E. Chigrinov, Nucl. Phys. A268, 513 (1976).
[10] H. W. Bertini, Phys. Rev. C 1, 423 (1970).
[11] I. Dostrovsky, Z. Fraenkel, and G. Friedlander, Phys. Rev. 116, 683 (1959).
[12] V. S. Butsev, Yu. K. Gavrilov, Dz. Ganzorig, S. M. Polikanov, and D. Chultem, Pis'ma Zh. Eksp. Teor. Fiz. 21, 400 (1975) [JETP Lett. 21, 182 (1975)].
[13] V. M. Abazov, S. R. Avramov, V. S. Butsev, E. P. Cherevatenko, D. Chultem, W. D. Fromm, Dz. Ganzorig, Yu. K. Gavrilov, and S. M. Polikanov, Nucl. Phys. A274, 463 (1976).
[14] H. D. Engelhardt, C. W. Lewis, and H. Ullrich, Nucl. Phys. A258, 480 (1976).
[15] H. S. Pruys, R. Engfer, R. Hartmann, U. Sennhauser, H.-J. Pfeiffer, H. K. Walter, J. Morgenstern, A. Wyttenbach, E. Gadioli, and E. Gadioli-Erba, Nucl. Phys. A316, 365 (1979).
[16] R. Beetz, F. W. N. de Boer, J. K. Panman, J. Konijn, P. Pavlopoulos, G. Tibell, K. Zioutas, I. Bergstrom, K. Fransson, L. Tauscher, P. Blum, R. Guigas, H. Koch, H. Poth, and L. M. Simons, Z. Phys. A286, 215 (1978).
[17] K. Chen, Z. Fraenkel, G. Friedlander, J. R. Grover, J. M. Miller, and Y. Shimamoto, Phys. Rev. 166, 949 (1968).
[18] K. Chen, G. Friedlander, G. D. Harp, and J. M. Miller, Phys. Rev. C 4, 2234 (1971).
[19] R. Gunnink and J. B. Niday, Lawrence Livermore Laboratory Report No. UCRL-51061 (1971–1972).
[20] S. Charalambus, Nucl. Phys. A166, 145 (1971).
[21] A. Wyttenbach, P. Baertschi, S. Bajo, J. Hadermann, K. Junker, S. Katcoff, E. A. Ermes, and H. S. Pruys, Nucl. Phys. A294, 278 (1978).
[22] G. Backenstoss, Annu. Rev. Nucl. Sci. 20, 467 (1970).
[23] D. K. Anderson, D. A. Jenkins, and R. J. Powers, Phys. Rev. 188, 9 (1969).
[24] C. W. de Jager, H. de Vries, and C. de Vries, At. Data and Nucl. Data Tables 14, 479 (1974).
[25] M. Leon, private communication.
[26] J. N. Ginocchio, Phys. Rev. C 17, 195 (1978).
[27] M. E. Nordberg, Jr., K. F. Kinsey, and R. L. Burman, Phys. Rev. 165, 1096 (1965).
[28] J. B. Cumming, P. E. Haustein, R. W. Stoenner, L. Mausner, and R. A. Naumann, Phys. Rev. C 10, 739 (1974).
[29] G. Rudstam, Z. Naturforsch. 21a, 1027 (1966).
[30] C. J. Orth, B. J. Dropesky, R. A. Williams, G. C. Giesler, and J. Hudis, Phys. Rev. C 18, 1426 (1978).
[31] P. Ebersol, B. Aas, W. Dey, R. Eichler, H. J. Leisi, W. W. Sapp, and H. K. Walter, Phys. Lett. 58B, 428 (1975).
[32] M. Hillman and Y. Eyal, Amer. Chem. Soc. 174th National Meeting, Chicago, 1977. Abstract No. 47, Nucl. Chem. and Technology Bulletin.